ELSEVIER

Journal of Nuclear Materials 297 (2001) 292–302

journal of nuclear materials

www.elsevier.com/locate/jnucmat

Precipitation of reoriented hydrides and textural change of α-zirconium grains during delayed hydride cracking of Zr–2.5%Nb pressure tube

Young Suk Kim *, Yuriy Perlovich [1], Margarita Isaenkova [1], Sung Soo Kim, Yong Moo Cheong

Zirconium Team, Korea Atomic Energy Research Institute, Yusong-gu, P.O. Box 105, Taejon 305-600, Republic of Korea

Received 4 December 2000; accepted 23 May 2001

Abstract

Cantilever beam (CB) specimens referred to as L90 and L60 with the notch directions tilted normal to, and at an angle of 60° to, the transverse direction of a cold-worked and annealed Zr–2.5%Nb pressure tube, respectively, were subjected to delayed hydride cracking (DHC) testing at 250°C. L60 specimen showed slanted growth of the DHC crack compared to L90 without tilting. An X-ray diffractometric study was carried out on the fractured surfaces of the two CB specimens after DHC testing. The δ-hydride phase was confirmed to sit on the fracture surface, demonstrating the growth of the DHC crack through fracturing of the reoriented hydrides. Furthermore, the texture of the reoriented hydrides was determined for the first time. Comparing the pole figures of the $\{1\,1\,1\}_{\delta\text{-hydride}}$ and the $(0\,0\,0\,1)_{\alpha\text{-zirconium}}$, it is concluded that the reoriented hydrides nucleate first of all at the α-zirconium grains. A change in the orientation of the α-zirconium grains, mainly by twinning on the $\{1\,0\,\bar{1}\,2\}$ planes, was demonstrated to occur during the propagation of the DHC crack. On the basis of the above findings, a mechanism of the DHC was discussed.

PACS: 62. 20. MK

1. Introduction

The current understanding of delayed hydride cracking (DHC) in zirconium alloys is that it occurs by reiterating the following three processes: diffusion of hydrogen toward the notch subjected to the highest tensile stress, precipitation of reoriented hydrides there and fracturing of hydrides. However, there are some issues to be resolved further: the constant velocity of DHC independent of applied stress intensity factor, K_I as long as K_I exceeds K_{IH}, a cause of the striation, the nucleation pattern of hydrides and anisotropic DHC behavior of Zr–2.5%Nb pressure tube with the direction. Since the reorientation of hydrides is a necessary condition for DHC, much attention must be paid to the habit plane of hydrides. This is because the hydride habit plane is the plane where the reoriented hydrides can nucleate under tensile loading. However, a review of the hydride habit plane of hydrides reveals that this issue is very controversial: the following lattice planes have been suggested as probable hydride habit planes:

1. the $\{1\,0\,\bar{1}\,0\}$ prismatic plane [1], the twinning plane of $\{1\,0\,\bar{1}\,2\}$, $\{1\,1\,\bar{2}\,1\}$ and $\{1\,1\,\bar{2}\,2\}$ [2], the $\{1\,0\,\bar{1}\,1\}$ pyramidal plane [3], the $(0\,0\,0\,1)$ basal plane [4], the $\{1\,0\,\bar{1}\,L\}$ and $\{1\,0\,\bar{1}\,7\}$ planes [5,6], or
2. the grain boundary or the inter-phase boundary [7–11].

By observing the growth pattern of the DHC crack with the notch direction, Kim demonstrates that the $\{1\,0\,\bar{1}\,7\}$

* Corresponding author. Tel.: + 82-42 868 2359; fax: +82-42 868 8346.

E-mail address: yskim1@kaeri.re.kr (Y.S. Kim).

[1] Visiting scientists from Moscow Engineering Physics Institute, Kashirskoe shosse 31, Moscow 115409, Russia.

0022-3115/01/$ - see front matter
PII: S0022-3115(01)00628-6

plane is the habit plane of the hydrides, thus governing the nucleation and growth pattern of the DHC crack [12].

Another thing to note is that plastic deformation of the α-zirconium ahead of the crack tip under applied tensile stress is relaxed to a certain degree with the maximum strain of 0.005 [13]. The cause of the stress relaxation is also controversial: compressive stress due to a volume difference between zirconium and zirconium hydride [14,15] or thermal creep [13]. When tensile loading is applied to the α-zirconium grains with the maximum basal poles parallel to it, then this may cause a change in the orientation of grains by twinning, thus resulting in a stress relaxation [16–18]. The twinning would occur due to no availability of the $\{10\bar{1}0\}$ slip planes in the tangential direction of the tube with the maximum of the (0 0 0 1) basal plane [12]. Hence, when the crack propagates by accompanied fracturing of hydrides, a change in the orientation of the α-zirconium grains would occur whose extent is the maximum especially ahead of the crack tip. Since the nucleation of hydrides is controlled by the availability of hydride habit planes, the change in the grain orientation ahead of the crack tip would affect the propagation of a DHC crack. However, it is not clear yet what is the effect of the textural change on the growth pattern of the DHC crack, or the nucleation pattern of hydrides ahead of the crack tip. Thus, it is very important to determine which process will occur first between the twinning and the precipitation of the hydrides on the hydride habit planes to gain a better understanding of DHC in the Zr–2.5%Nb pressure tube.

The objective of this study is to investigate the nucleation pattern of hydrides and the effect of textural change in the α-zirconium accompanied by delayed cracking of a Zr–2.5%Nb pressure tube. To this end, the texture pole figures of reoriented hydrides on the fracture surface of the cantilever beam (CB) specimen were analyzed for the first time with X-ray. In addition, the textural change of the α-zirconium grains was evaluated by comparing textures before and after fracture of the CB specimen taken from the Zr–2.5%Nb pressure tube.

2. Experimental procedures

Two kinds of CB specimens taken from a typical cold-worked and annealed Zr–2.5%Nb pressure tube

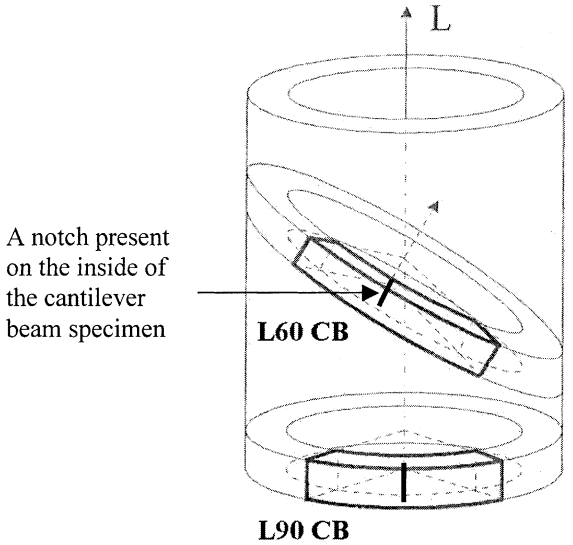

Fig. 1. CB specimens of L60 and L90 with notches inclined at angles of 60° and 90° to the longitudinal direction.

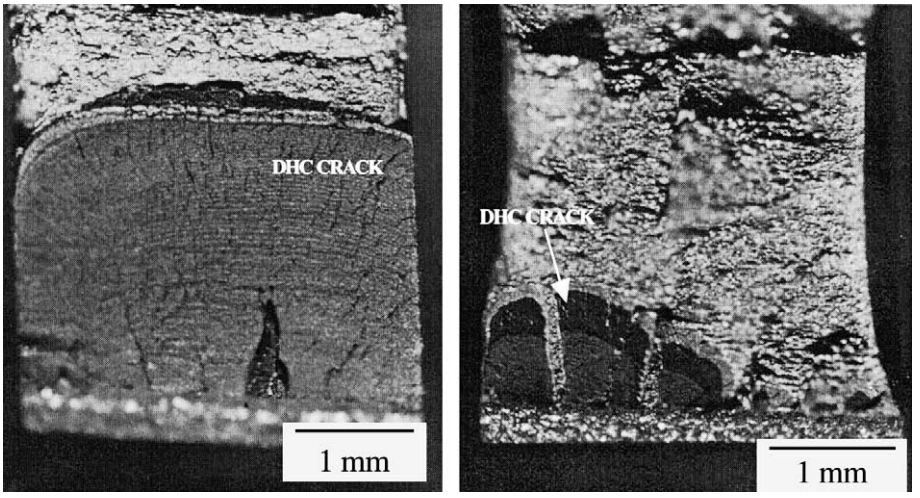

Fig. 2. DHC crack growth pattern of (a) L90 and (b) L60 CB specimens at 250°C.

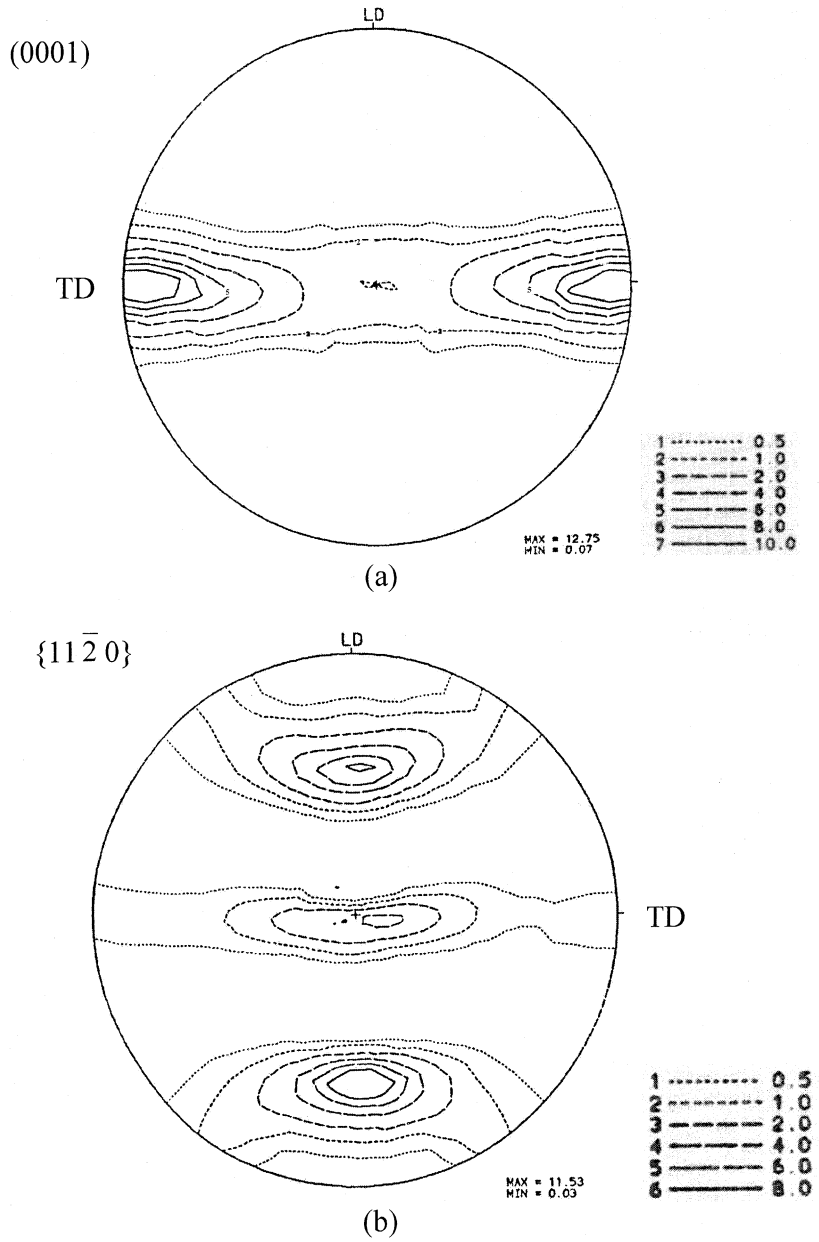

Fig. 3. Direct pole figures of (a) (0 0 0 1) and (b) $\{1\,1\,\bar{2}\,0\}$ for the Zr–2.5%Nb tube with the radial direction in the center.

[19] were subjected to DHC testing at 250°C after charging of hydrogen of 60 ppm H electrolytically as shown in Fig. 1. Here, L90 and L60 specimens are the ones to be cut off normal to, and at an angle of 60° to, the longitudinal direction of the Zr–2.5%Nb tube, respectively, to have the notch direction lying normal to, and at an angle of 60° to, its transverse direction. Detailed procedures of DHC testing have already been reported elsewhere [19,20]. Further, the tube sections perpendicular to the longitudinal, transverse and radial directions, are referred to as the longitudinal, transverse and radial sections, respectively. A sharp notch was made on the internal surface of the CB specimens so that the notch plane coincided with the transverse section for the L90 specimen and tilted from the transverse section by 30° for the L60 specimen. Thus, the L90 and L60 CB specimens were subjected to tensile loading at angles of 0° and 30° to the transverse direction, respectively. The stress intensity coefficient K_I at the notch tip was set to 17 MPa $m^{1/2}$ at the beginning and decreased to less than

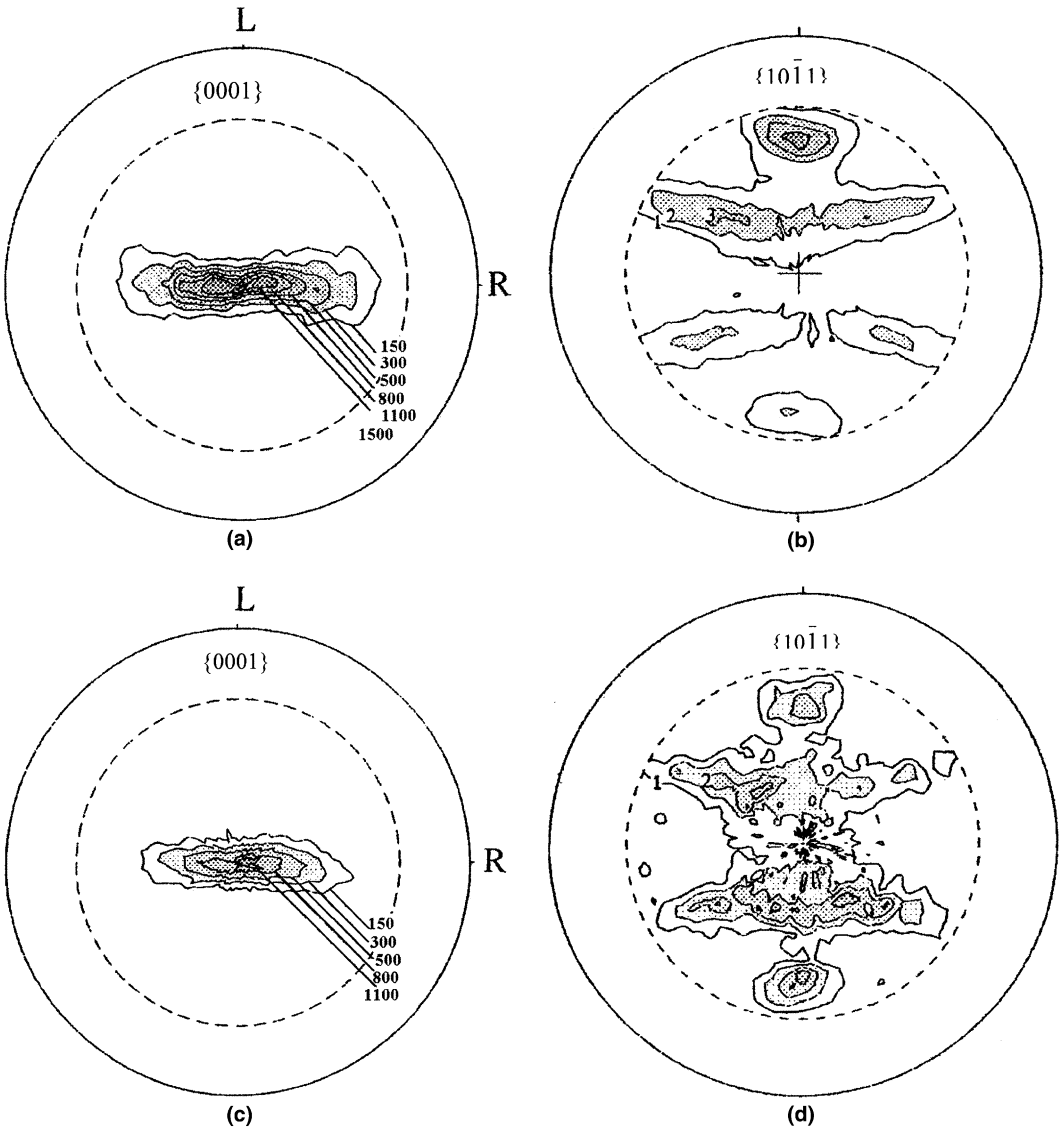

Fig. 4. Direct pole figures of (0 0 0 1) and $\{1\,0\,\bar{1}\,1\}$ obtained at a distance of 20 mm from the fractured surface (a,b) and at the fractured surface (c,d).

15 MPa $m^{1/2}$ with the crack propagation [20]. The crack growth was monitored by an acoustic emission method [19,20].

After DHC testing, the CB specimens were broken up into two parts whose fracture surfaces were subjected to X-ray diffraction analysis to investigate the texture of hydrides sitting on the fractured surface and the reorientation of α-zirconium grains accompanied by DHC. The thickness of the plastically deformed layer, affecting the intensity of X-ray reflection, varies with Bragg's angle 2θ and tilt angle α, being about 15–20 μm with the Cu K_α radiation on zirconium alloys [21]. This is comparable with the thickness of the plastic deformation zone in brittle fracture [22]. Thus, an X-ray study of the fracture surfaces seems to be sufficiently sensitive enough to identify the effect of plastic deformation accompanied by fracture or the propagation of the DHC crack. An automated X-ray diffractometer (Siemens D5000) with a position sensitive detector (PSD) and the Cu K_α radiation was used so that the X-ray data are characterized with relatively high statistical significance and therefore can be considered reliable with high confidence. Based on the diffraction spectra obtained, the inverse pole figures were constructed. The complete pole figures were reconstructed using orientation distribution functions (ODF) [23,24] obtained from the incomplete

pole figures determined experimentally. Besides the fracture surface, the section at a distance of 20 mm from it, was examined to represent the initial texture pole figures of zirconium grains before fracture.

3. Results and discussion

3.1. Textural change of α-zirconium grains accompanied by delayed hydride cracking of the Zr–2.5%Nb tube

Fig. 2 shows growth patterns of the DHC crack on the fractured surfaces of the L90 and L60 CB specimens. The L90 specimen had the DHC crack grown fully along the notch plane (the radial–longitudinal plane). In contrast, the L60 specimen did not have the DHC crack grown fully from the notch but tiled growth of the DHC crack initiated locally at a part of the initial notch.

Since the C.W. Zr–2.5%Nb tube has a strong tangential texture as shown in Fig. 3, tensile loading along the tangential direction applied during DHC testing seems to cause a textural change in α-zirconium grains during the propagation of DHC crack by twinning at the planes $\{10\bar{1}2\}$. This is because the α-zirconium grains subjected to tensile stress along the basal normal can deform only by twinning [16–18]. Fig. 4 shows the (0 0 0 1) and $(10\bar{1}1)$ incomplete pole figures of the L90 specimen obtained at the fractured surface and at a distance of 20 mm from it, representing the incomplete pole figures before its fracture. Here, the incomplete pole figures are the ones made from the limited intensities obtained by tilting the specimen from 0° to 60° or 70° at the maximum to the X-ray beam. It should be noted that the line intensity described in Fig. 4 represents the measured line intensity rather than the pole density. To clearly identify a change in the intensity and distribution of the (0 0 0 1) pole figure accompanied by fracture, the contours of the intensity ratio of the (0 0 0 1) pole figures before and after the fracture were plotted with an angular radius of 45° as shown in Fig. 5. As expected, a textural change occurred by twinning, thus decreasing the intensity of the (0 0 0 1) pole figure. The textural change was more clearly illustrated by comparing the inverse pole figures of the L90 specimen before and after fracture. Fig. 6 shows the inverse pole figures of the L90 specimen (a) before and (b) after the fracture, and (c) shows a change in the pole densities accompanying the fracture in the stereographic sector. The strong texture maximum of (0 0 0 1) pole at the $\langle 0001 \rangle$ axis decreased, yielding a relatively weak maximum near the center of the sector toward the $(10\bar{1}2)$ pole. In other words, the density of the prismatic planes into the transverse section of the L90 specimen became larger after the fracture, as a result of twinning on the $\{10\bar{1}2\}$ planes. The textural change accompanied by fracture was also confirmed from the $\{10\bar{1}1\}$ pole figures before and after the fracture of the L90 CB specimen, revealing more uniform redistribution of the $\{10\bar{1}1\}$ pyramidal pole toward the center of the transverse section.

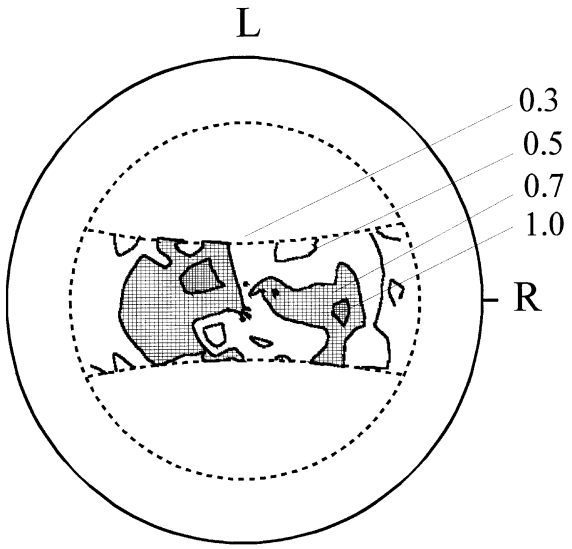

Fig. 5. Change in the intensity ratio of the (0 0 0 1) basal pole, $I_1(\varphi,\psi)/I_0(\varphi,\psi)$, where I_1 and I_0 are the intensities of the line (0 0 0 2) obtained at the fractured surface and at a distance of 20 mm from it. The shaded zones correspond to little change in the intensity of the (0 0 0 2) pole under the angular radius of 45°.

3.2. Textural analysis of the hydride on the fracture surface

To identify the presence of hydrides on the fracture path of DHC, the diffraction spectrum of the fractured surface was compared with that of the bulk region of the L90 specimen as shown in Fig. 7. The diffraction spectrum of the bulk region was taken from a transverse section at a distance of 20 mm from the fracture surface. On the fractured surface only were observed two additional lines of δ-hydrides corresponding to the (1 1 1) and (2 2 0) planes besides the lines of the α-zirconium (Fig. 7(b)). These results demonstrate that the reoriented hydrides with mainly $\{111\}$ poles precipitate on the fracture surface.

A question is whether the reoriented hydrides observed only at the fracture surface precipitate in the initial α-zirconium grains or the twinned grains since a textural change by twinning is accompanied during DHC testing. As a clue to this question, the $\{111\}$ incomplete pole figures of the reoriented δ-hydrides were determined for the first time. Fig. 8 shows the $\delta\{111\}$ pole figures of the reoriented hydride taken from the fractured surfaces of the L90 and L60 specimens. Both the $\delta\{111\}$ pole figures indicate a similar distribution and splitting of the texture maxima at the central region.

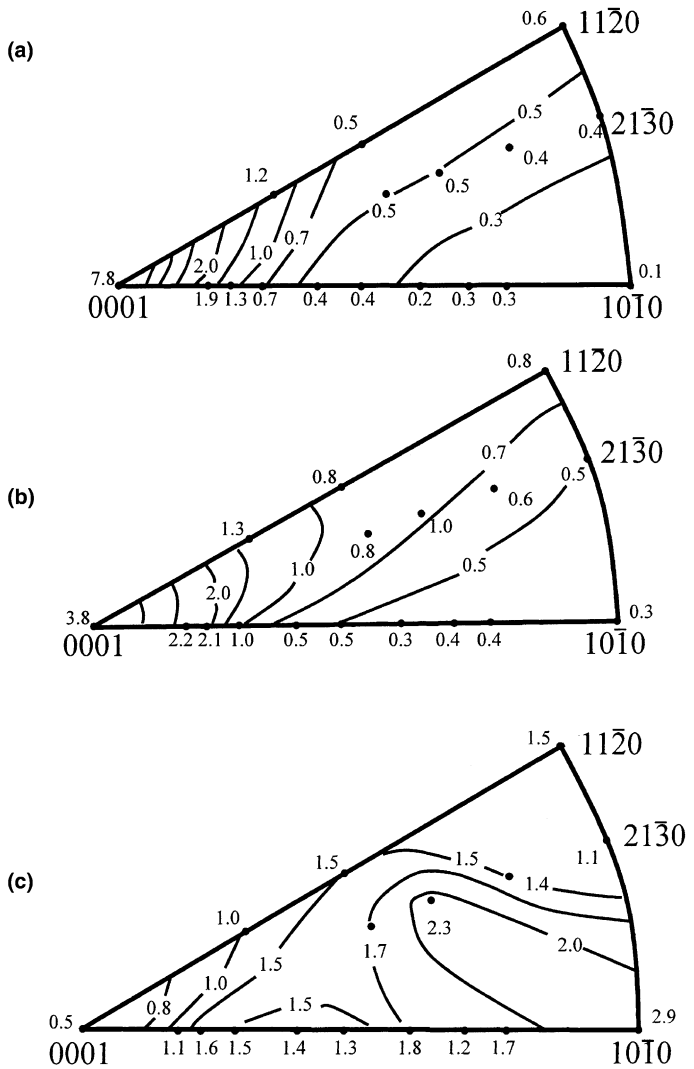

Fig. 6. Inverse pole figures of L90 CB specimen obtained (a) at a distance of 20 mm from fractured surface, (b) at the fractured surface and (c) a change in the pole densities accompanied by DHC.

Compared with the (0 0 0 1) pole figure before the fracture as shown in Fig. 4, the {1 1 1} pole figure pattern of the reoriented δ-hydrides for the L90 and L60 specimens was found to be almost the same as the (0 0 0 1) pole figure pattern of the α-zirconium grains before the fracture. This is another example of confirming the well-known orientation relationship between hydride and α-zirconium grain of $(1\,1\,1)_{\delta}\|(0\,0\,0\,1)_{\alpha\text{-zirconium}}$ [25]. It is to be noted that this orientation relationship holds for the reoriented hydride. Thus, we can conclude that most reoriented hydrides precipitate in the untwinned α-zirconium grains keeping the initial texture. This suggests that the nucleation of hydrides occurs first in the α-zirconium grains and then a textural change probably by twinning is accompanied by fracturing of the nucleated hydrides corresponding to the propagation of the DHC crack.

Since no diffraction lines of hydrides were observed on the transverse section 20 mm from the fracture surface, the δ{1 1 0} lines must also come from the reoriented hydrides. Since the δ{1 1 1} pole figures have a distribution whose maximum roughly corresponds to the transverse direction, not all the reoriented hydrides form parallel to the fracture surface but there are a few hydrides tilted at some angles from it. Especially, the δ{1 1 1} tilting at 35° from the fracture surface appears to yield a diffraction line equal to the {1 1 0} planes because the minimum angle between the ⟨1 1 1⟩ and ⟨1 1 0⟩ axes is 35° in the cubic lattice. This can explain much lower intensity of the {2 2 0} planes compared to the

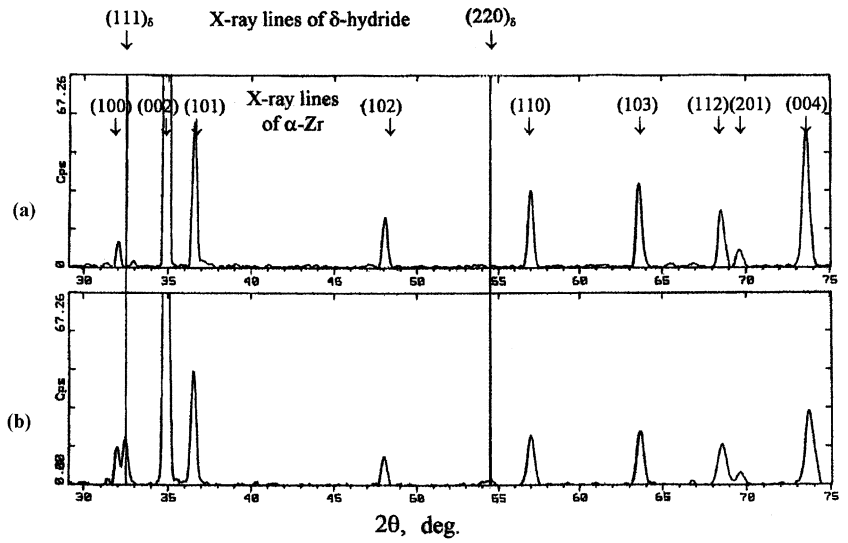

Fig. 7. XRD patterns determined (a) at a distance of 20 mm from the fractured surface and (b) at the fractured surface of L90 CB specimen after DHC testing at 250°C, demonstrating the hydrides sitting on the fractured surface.

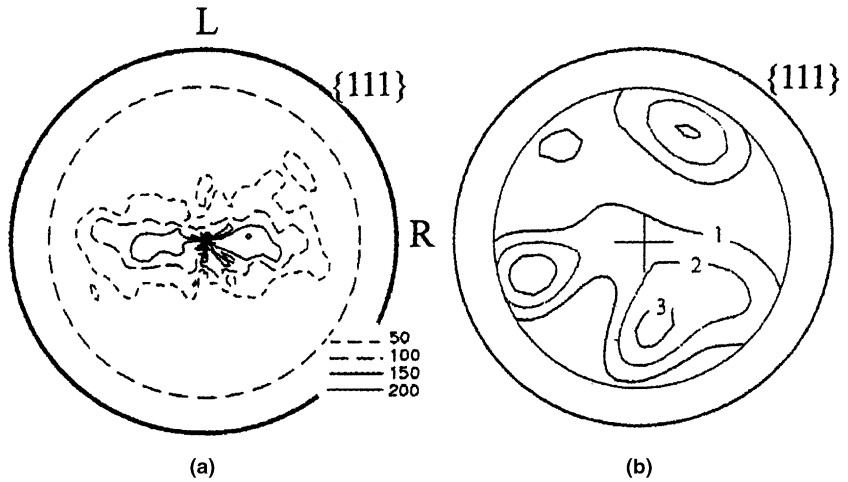

Fig. 8. (1 1 1) pole figures of hydrides on the fractured surface of (a) L90 and (b) L60 specimens.

{1 1 1} planes as shown in Fig. 7. Likewise, the δ{1 1 1} hydrides whose ⟨1 1 1⟩ axes are tilted at 11.4° from the transverse direction have the {2 2 1} plane parallel to the fracture surface. Even though a significant fraction of hydrides has this orientation, we cannot observe any X-ray reflection lines from these hydrides. It is because the X-ray line (2 2 1) cannot appear under the copper radiation in accordance with the Bragg rule. Thus, the Bragg rule allows one to observe only two orientations of hydrides within the texture maximum in the (1 1 1) pole figure for the fracture surface perpendicular to the transverse direction. In short, there are only two lines of δ{1 1 1} that can meet the Bragg rule, suggesting that the {2 2 0} line corresponds to the δ{1 1 1}.

As a conclusion, most reoriented hydrides of the {1 1 1} poles precipitate first of all in the undeformed grains or the grains keeping the initial texture of the (0 0 0 1) pole. Thus, the region where the reoriented hydrides can precipitate would correspond to the shaded area illustrated in Fig. 5 because the shaded area is the one with a slight decrease or no change in the initial pole density during fracture of the L90 specimen. This strongly suggests that there is a limited area where hydride precipitates can nucleate even at the fractured surface, whose pole is not parallel to the transverse direction but is tilted at an angle of 15–30° toward the radial direction from the transverse direction.

3.3. Understanding of DHC process in Zr–2.5%Nb pressure tube

Based on the above results, a better understanding of DHC of the Zr–2.5%Nb tube can be gained. Under tensile loading, hydrogen diffuses toward the notch tip region subjected to the highest tensile stress, causing the nucleation of reoriented hydrides there and also its textural change by plastic deformation. However, the first process to occur is the former. This is based on the fact that the $\{1\,1\,1\}$ pole figure pattern of the hydrides precipitated at the notch tip looks after that of the $(0\,0\,0\,1)$ pole figure of the initial α-zirconium matrix as shown in Figs. 4 and 8. Thus, nucleation of the reoriented hydrides occurs in a limited area keeping the initial texture ahead of the notch as shown in Fig. 5, which has brittle fracture of the hydrides with little plastic deformation of the α-zirconium matrix during the propagation of a DHC crack. Since the DHC crack grows through fracturing of the hydrides with splitting peaks tilting toward both sides of the radial direction from the transverse direction, the nucleation pattern of the DHC crack will take a similar shape as that (Fig. 5). Fig. 9, showing the splitting nucleation of DHC cracks at the notch, provides decisive evidence. Thus, it is concluded that the hydrides nucleate at the α-zirconium grains keeping the initial texture, and maintaining the orientation relationship of $\{1\,1\,1\}_\delta \| (0\,0\,0\,1)_\alpha$.

When the DHC crack propagates, plastic deformation of the α-zirconium matrix is accompanied around the cracked area, which is the most striking ahead of the cracking hydride. This will cause a textural change by twinning as shown in Figs. 4–6, preventing the reoriented hydrides from nucleating ahead of the crack tip because of no available hydride habit planes. Thus, this will have an effect on stopping continuous propagation of the DHC crack. Further, the deformed area by twinning must have a ductile fracture pattern as opposed to a brittle fracture pattern by fracturing of hydrides. Thus, the deformed area appears as a line, called the striation, as shown in Figs. 10 and 11. This can explain why the DHC process occurs discontinuously.

Since the nucleation and growth of reoriented hydrides on the $\{1\,0\,\bar{1}\,7\}$ habit planes govern DHC of Zr–2.5%Nb alloy [12], we also investigated the $\{1\,0\,\bar{1}\,7\}$ pole figure of the Zr–2.5%Nb tube. Fig. 12 shows the $\{1\,0\,\bar{1}\,7\}$ complete pole figure that was reconstructed using orientation distribution functions from measured five incomplete pole figures [22]. The maxima of the $\{1\,0\,\bar{1}\,7\}$

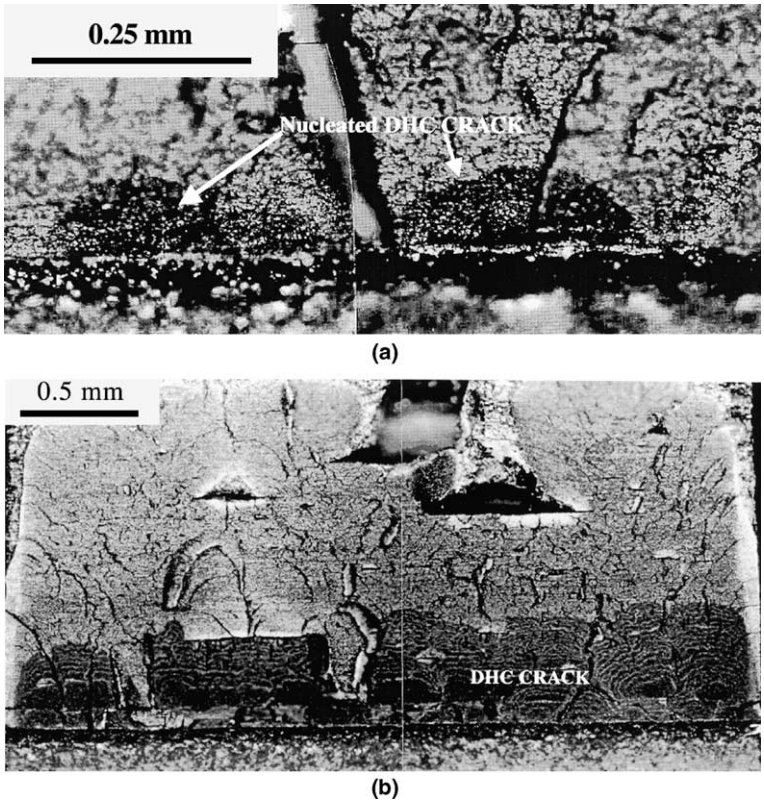

Fig. 9. (a) Splitting nucleation of DHC cracks at the notch and (b) growth of nucleated cracks over the whole breadth of the specimen.

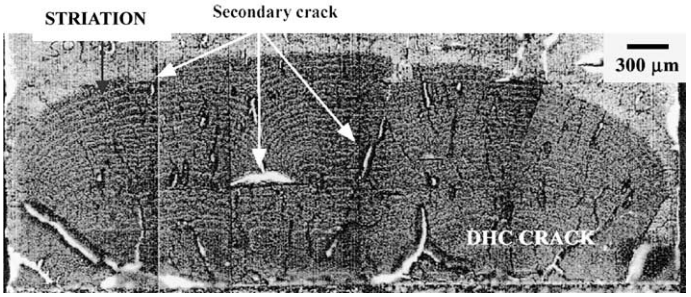

Fig. 10. Typical striation pattern and the secondary hydride cracking on the fractured surface of L90 CB specimen after DHC testing, at 250°C.

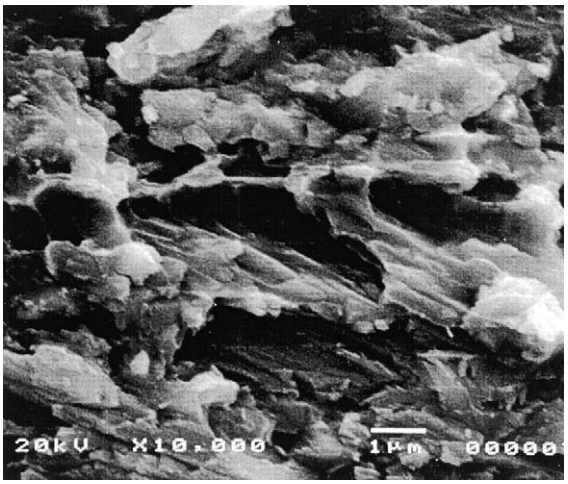

Fig. 11. Enlarged microstructure of the striation observed on the fractured suface after DHC testing.

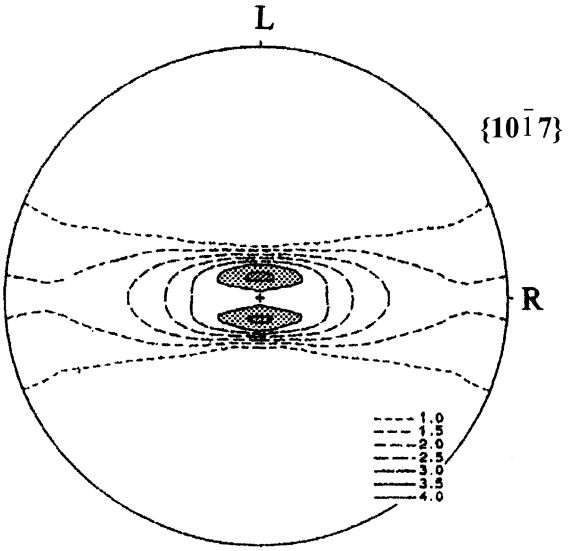

Fig. 12. $\{10\bar{1}7\}$ pole figures on the transverse section of the Zr–2.5%Nb pressure tube before fracture.

poles shifted toward the longitudinal direction from the transverse direction by approximately 15°, where the reoriented hydrides nucleate in the first place. Therefore, when the notch is lying parallel to the radial direction as in the L90 specimen, the DHC crack may grow parallel to the radial direction on a macroscopic scale as shown in Fig. 2(a). In contrast, when the notch plane is lying 30° from the tangential direction as in the L60 specimen, the DHC crack cannot grow along the radial direction because of no availability of the habit plane. Thus, the DHC crack would slant toward the habit plane away from the notch plane, which is inclined at an angle of 45° considering the pole figures of the $\{10\bar{1}7\}$ habit plane. This is the cause of tilted growth of the DHC crack as appeared on the fractured surface of the L60 specimen (Fig. 2(b)).

However, when looking at the growth pattern of the DHC crack in the L90 specimen in more detail, the DHC crack may not grow along the radial direction but slant toward the longitudinal direction 15° away from the notch plane. This was evidenced by a DHC fracture pattern taken from the L90 specimen after DHC testing as shown in Fig. 13, where two DHC cracks have grown at different angles to the notch plane. There is more evidence for the cracks tilting toward the longitudinal direction to the cracking plane. Fig. 14 shows a cross-sectional plot on the contrast and gray-scale elevation image of the fractured surface of the L90 specimen made by confocal optics based on scanning laser microscope. The cross-sectional plot along the cracking direction A–A shows slanted growth of the DHC crack. Furthermore, the deviation of the growing hydrides from the radial–longitudinal plane, or the cracking plane, leads to slowing down of the crack velocity in contrast with the case of hydrides growing in parallel with the cracking plane [26,27].

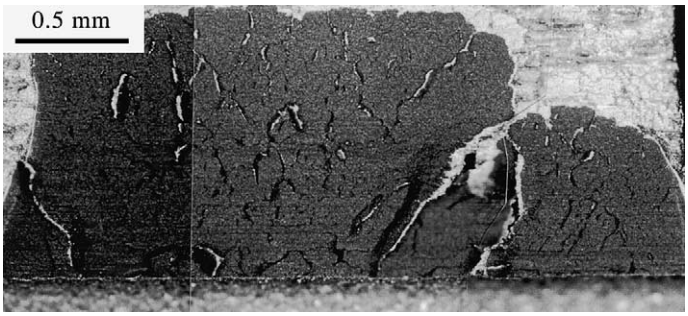

Fig. 13. Growth of the DHC cracks with different angles to the notch plane.

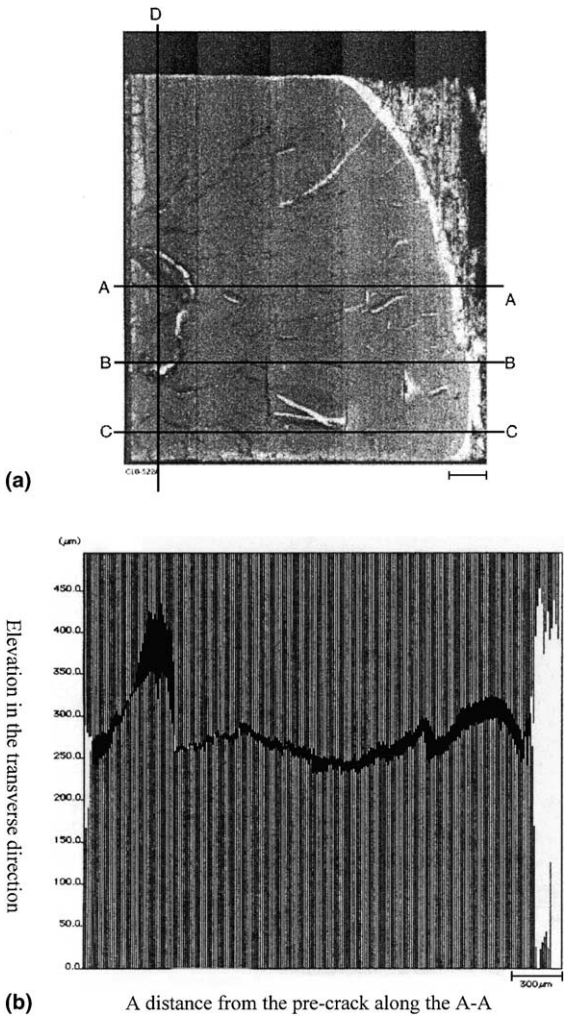

Fig. 14. (a) Contrast and gray-scale elevation image made by confocal optics based scanning laser microscope and (b) the cross-sectional plot along the A–A line on the contrast and gray-scale image.

4. Conclusion

The L90 specimen had a DHC crack grown fully along the notch plane (the radial–longitudinal plane) while the L60 specimen with the notch plane tilted at an angle of 30° to the longitudinal direction had tilted growth of the DHC crack initiated locally at a part of the initial notch. The δ-hydride phase was observed using X-ray on the fracture surfaces of the L90 specimen subjected to DHC testing at 250°C. Furthermore, the texture of the reoriented hydrides was determined for the first time. The $\{1\,1\,1\}$ pole figure of the hydride showed a similar pattern of $(0\,0\,0\,1)$ pole figure of the α-zirconium matrix. Thus, it is concluded that the reoriented hydrides nucleate first of all at the α-zirconium grains, keeping the initial texture. During the propagation of the DHC crack, the α-zirconium grains reoriented by twinning in a thin plastic deformation zone near the fracture surface, which is the highest ahead of the nucleated hydride. This reorientation of the α-zirconium grains ahead of the precipitated hydride seems to prevent hydrides from precipitating continuously, resulting in stopping the propagation of the DHC crack. This area with the reoriented α-zirconium grains likely corresponds to the striation often observed in the fractured surfaces of the specimen after DHC testing. The $\{1\,0\,\bar{1}\,7\}$ pole figure of the Zr–2.5Nb pressure tube was presented. Since the $\{1\,0\,\bar{1}\,7\}$ planes acting as the hydride habit plane during DHC tilted around by 15° toward the longitudinal direction from the transverse direction, this can explain the tilted growth of the DHC crack away from the longitudinal–radial section.

Acknowledgements

This work was has been carried out as a part of the Nuclear R&D program supported by Ministry of Science and Technology, South Korea. In addition, the financial support of the Korea Institute of Science and Technology, Evaluation and Planning is acknowledged.

One of the authors would like to express his sincere thanks to Y.W. Kim and T. Kobayashi (SRI International) for the examination of the fractured surfaces using a scanning laser microscope.

References

[1] J.P. Langeron, P. Lehr, Rev. Metall. 155 (1958) 901.
[2] F.W. Kunz, A.E. Bibb, Trans. AIME 218 (1960) 133.
[3] D.G. Westlake, E.S. Fisher, Trans. AIME 224 (1962) 254.
[4] R.P. Marshall, J. Nucl. Mater. 24 (1967) 49.
[5] W.J. Babyak, Trans. AIME 239 (1967) 232.
[6] C. Roy, J.G. Jacques, J. Nucl. Mater. 31 (1969) 233.
[7] V. Perovic, G.C. Weatherly, C.J. Simpson, Acta Metall. 31 (1983) 1381.
[8] V. Perovic, G.C. Weatherly, J. Nucl. Mater. 126 (1984) 160.
[9] V.S. Arunachalam, B. Lentinen, G.J. Ostberg, J. Nucl. Mater. 21 (1967) 241.
[10] G.F.R. Ambler, J. Nucl. Mater. 28 (1968) 237.
[11] P. Gangli, J. Root, R. Fong, Can. Metall. Q. 34 (1995) 211.
[12] Y.S. Kim, S.C. Kwon, S.S. Kim, J. Nucl. Mater. 280 (2000) 304.
[13] B. Leitch, N. Christodoulou, J. Root, in: Transactions of the 15th International Conference on Structural Mechanics in Reactor Technology (SMiRT-15), vol. XII, 1999, p. 133.
[14] S.Q. Shi, M.P. Puls, J. Nucl. Mater. 208 (1994) 232.
[15] Y.S. Kim, Y.G. Matvienko, Y.M. Cheong, S.S. Kim, S.C. Kwon, J. Nucl. Mater. 278 (2000) 251.
[16] E. Tenkhoff, Verformungsmechanismen Textur und Anisotropie in Zirkonium und Zircaloy, Materialkundlich-Technische Reihe, 5, Gebruder Borntraeger, Berlin, 1980, 79 S.
[17] I.V. Matcegorin, A.A. Rusakov, A.I. Evstyukhin, in: V.S. Emelyanov (Ed.), Metallurgy and Metal Science of Pure Metals, N 14, Atomizdat, Moscow, 1980, p. 39 (in Russian).
[18] M. Isaenkova, Yu. Perlovich, Phys. Met. Metallogr. (USSR) (UK) 71 (1991) 81.
[19] S.S. Kim, S.C. Kwon, Y.S. Kim, J. Nucl. Mater. 273 (1999) 52.
[20] Y.S. Kim, KAERI Technical Report, KAERI/TR-1329/99, 1999.
[21] Yu. Perlovich, M. Isaenkova, V. Goltzev, J. Phys. IV, Colloque C6 (supplement au J. Phys. III) 6 (1996) 335.
[22] G. Klevtsov, Yu. Perlovich, V. Eessnko, Ind. Lab. (Russia) (USA) 59 (1994) 774.
[23] M.M. Borodkina, E.N. Spector, X-ray Analysis of Texture in Metals and Alloys, Metallurgia, Moscow, 1981, p. 271 (in Russian).
[24] L. Wcislak, H.J. Bunge, Texture Analysis with a Position Sensitive Detector, Cuvillier, Goettingen, 1996, p. 215.
[25] J.S. Bradbrook, G.W. Lorimer, N. Ridley, J. Nucl. Mater. 42 (1972) 142.
[26] S. Sagat, C.E. Coleman, M. Griffiths, B.J.S. Wilkins, in: Proceedings of the 10th International Symposium on Zirconium in the Nuclear Industry, ASTM STP 1245, 1994, p. 35.
[27] Y.S. Kim, S.S. Kim, D.J. Oh, S.C. Kwon, K.S. Im, in: Proceedings of the 2nd Symposium on Material and Fracture Mechanics, Korea Mechanical Engineering Society, 2000, p. 218.